Electric Vehicles Charging Time Constrained Deliverable Secondary Frequency Regulation Provision

Jinning Wang, *Student Member, IEEE,* Fangxing Li, *Fellow, IEEE,* Xin Fang, *Senior Member, IEEE,* Wenbo Wang, *Member, IEEE,* Hantao Cui, *Senior Member, IEEE,* Qiwei Zhang, *Student Member, IEEE,* Buxin She, *Student Member, IEEE*

***Abstract*—Electric Vehicle (EV) aggregation is a promising technique to provide secondary frequency regulation (SFR) in highly renewable energy-penetrated power systems. Equipped with energy storage devices, EV aggregation can provide reliable SFR. However, the main challenge is guaranteeing reliable intra-interval SFR capacities and inter-interval delivery following the automatic generation control (AGC) signal. Furthermore, aggregated EV SFR provision will be further complicated by the EV charging time anxiety because SFR provision might extend EV's charging time. This paper proposes a deliverable EV SFR provision with a charging time-constrained control strategy. First, a charging time-constrained EV aggregation is proposed to address the uncertainty of EV capacity based on the state space model considering the charging time restriction of EV owners. Second, a real-time economic dispatch and time domain simulation (RTED-TDS) co-simulation framework is proposed to verify financial results and the dynamic performance of EV SFR provision. Last, the proposed charging time-constrained EV aggregation is validated on IEEE 39-bus system. Results demonstrate that with the charging time-constrained EV aggregation, the system's dynamic performance can be improved with a marginal total cost increase. More importantly, the charging time constraint can be respected in the proposed EV aggregation SFR provision control.**

***Index Terms*—Secondary frequency regulation, electric vehicle aggregation, charging time anxiety, state-space modeling, co-simulation**

NOMENCLATURE

Indices and Sets

Ω_B	Set of all buses
Ω_E	Set of all EV aggregators
Ω_G	Set of all generators
Ω_K	Set of all branches
Ω_T	Set of all RTED intervals

Parameters and Variables

$\Delta D_t^U/\Delta D_t^D$	Demanded RegUp/Dn capacity at time t
ρ_g^U/ρ_g^D	Ramp-up/-down limit (MW/min) of generator g
$c_{e,t}^U/c_{e,t}^D$	Price ($/MWh) of EV aggregator g for RegUp/Dn at time t
$c_{g,t}$	Bid price ($/MWh) of generator g at time t
$c_{g,t}^U/c_{g,t}^D$	Price ($/MWh) of generator g for RegUp/Dn at time t
D_b	Load demand (MW) of bus b
$P_{g,t}^{\text{sch}}$	Scheduled power generation (MW) of generator g at time t
$P_{l,k}$	Line flow through branch k
$R_{e,t}^U/R_{e,t}^D$	RegUp/Dn capacity (MW) of EV aggregator e at time t
$R_{g,t}^U/R_{g,t}^D$	RegUp/Dn capacity (MW) of generator g at time t

Jinning Wang, Fangxing Li, Qiwei Zhang, and Buxin She is with the Department of Electrical Engineering and Computer Science, University of Tennessee, Knoxville, TN 37996 USA.

Xin Fang is with the Department of Electrical and Computer Engineering, Mississippi State University, Starkville, MS 39762, USA. (e-mail: xfang@ece.msstate.edu).

Wenbo Wang is with Grid Planning and Analysis Center, National Renewable Energy Laboratory, Golden, CO 80401 USA.

Hantao Cui is with the Department of Electrical and Computer Engineering, Oklahoma State University, Stillwater, OK 74077 USA.

I. INTRODUCTION

WITH the increasing integration of variable renewable energy generation involving solar power and wind power [1], [2], the stress confronted to system frequency regulation increases substantially. Secondary frequency regulation (SFR) is an essential grid service that maintains the power balance and regulates system frequency to its set value. To mitigate the system frequency fluctuation caused by load and variable power generation, the requirements of SFR increase remarkably. However, given the gradual retirement of conventional generators, the controllable resources in the generation mix are continuously decreasing. Therefore, it is essential to find more alternative energy resources that can provide reliable SFR for the future power system with high requirements on frequency regulation. Regarding the SFR, the ancillary market is usually co-optimized with the energy market [3], [4] to maintain the inter-interval power balance. Once the procurement of SFR is settled down, the automatic generation control (AGC) units are responsible for delivering the intra-interval regulating power. Variable generation providing SFR brings the gap between the intra-interval procurement and the inter-interval delivery. Distributionally robust chance-constrained modeling is applied to procure intra-interval SFR capacities and provide deliverable inter-interval SFR services [5].

Equipped with energy storage devices, Electric Vehicles (EV) can exchange power with the power grid in two directions to provide vehicle-to-grid services [6], [7]. Since the capacity of a single EV is limited, aggregation of a

large population of EVs was developed to provide helpful frequency service [8], [9]. The challenge of modeling EV aggregators is the randomness brought by traveling behaviors and heterogeneous parameters of numerous EVs. The EVs can be classified based on their SOC level and thus can be described as a Markov process and modeled as a state space transition model based on Markov theory [10], [11]. Further, the communication burden is significantly relieved because the control signal is designed for groups rather than every EV. However, the studies mentioned above focused on the continuous manner of AGC control while ignoring the procurement and delivery process of the SFR [5], [12], [13]. In addition, charging anxiety, or named range anxiety [14], is a barrier that impedes EVs from participating in the SFR program because the energy consumed by the SFR will result in an increased charging time. The issue of time anxiety is presented and alleviated by considering the patterns of EV behaviors [15]. Further, the aggregated anxiety concept is proposed, and a model-free deep reinforcement learning method is developed to optimize the charging schedule [16]. However, the methods discussed above are toward a single EV. They are not applicable in EV providing SFR because the relative significant AGC power signal requires aggregation of numerous EVs. In summary, the challenges for EV providing SFR can be summarized as follows:

1) It should be addressed that EV randomness involves not only the procurement stage but also the delivery stage.
2) The increased charging time should be constrained to secure the EV owners' preference.
3) The comprehensive assessment of EV SFR provision involves economic perspective and dynamic performance.

Based on the motivation, this paper proposes an increased charging time-constrained and deliverable SFR strategy from EVs. The EV aggregation is modeled based on state space modeling to effectively estimate the available SFR capacity in the procurement stage and reliably deliver the AGC signal in the real-time operation stage. Through the RTED-TDS co-simulation, the proposed strategy is validated to provide deliverable SFR service while the increased charging time is constrained to secure the EV owner's preference. The major contributions of this paper are summarized bellows:

1) The problem of EVs participating in the RTED to provide SFR is decoupled into dispatch modeling and EV aggregator modeling, where the procured capacity from EVs can be reliably delivered in the real-time operation stage.
2) The increased charging time caused by the SFR services is translated into an action counter and is constrained by the EV owner's tolerance.
3) A hybrid OPF structure is proposed in the RTED-TDS co-simulation for the frequency regulation studies, where the transition from dispatch to dynamic is secured, and the modeling complexity is reduced. With the hybrid OPF structure, the proposed RTED-TDS co-simulation allows fast prototyping of dispatch-dynamic co-simulation studies.
4) EV providing deliverable SFR is verified using the proposed RTED-TDS co-simulation. The results show that the dynamic system performance is improved with the charging time constraints, and the EV owners' tolerance of increased charging time is obeyed.

The rest of this paper is organized as follows: Section II discusses the charging time-constrained EV aggregator modeling; Section III presents the problem formulation of EV providing SFR in the RTED and the framework of RTED-TDS co-simulation; Section IV verifies the proposed charging time-constrained EV control strategy using the proposed RTED-TDS co-simulation on the IEEE 39-bus system; and Section V concludes this paper.

II. Charging Time Constrained EV Aggregator Modeling

This section introduces the charging time-constrained EV aggregator modeling, including the charging time-constrained SFR capacities estimation and the EV control for real-time AGC power delivery.

A. Overview State Space Model Based EV Aggregator

The uncertainties of EVs come from heterogeneous parameters and random traveling behaviors. Various EV models bring heterogeneous parameters, including capacity Q, charging efficiency η_c, and discharging efficiency η_d. An EV must plug in if the SOC level reaches a low level after a trip, which consists of random traveling behaviors involving arriving time t_s, departure time t_f, initial SOC level SOC_i, and demanded SOC level SOC_d.

To address the uncertainties of EV for frequency service, a state space model-based EV aggregator [17] is proposed. The proposed model applied the Markov state transition method to predict and control the EV aggregator status. Here we will overview the philosophy of the state space model-based EV aggregator.

An EV in a charging station can have three service actions, i.e., charging status, idle status, and discharging status. The regulation services can be achieved by switching EVs between different statuses. Further, categorizing the SOC level of the EV as N_s levels, an EV can be classified into a specific status out of $3N_s$. After a while, the EV will transit into a new status. Further, the status of a population of EVs can be described by a $3N_s \times 1$ vector that each element represents the proportion of EVs in a situation out of total EVs. Therefore, an EV population can be described with the state transition probability as shown in Eqn (1).

$$\begin{cases} \mathbf{x}(k+1) = \mathbf{A}\left(\mathbf{x}(k) + \mathbf{B}\mathbf{u}(k) + \mathbf{C}\mathbf{v}(k)\right) \\ y(k) = \mathbf{D}\left(\mathbf{x}(k) + \mathbf{B}\mathbf{u}(k) + \mathbf{C}\mathbf{v}(k)\right) \end{cases} \tag{1}$$

where vectors $\mathbf{x}(k)$ and $\mathbf{x}(k+1)$ are the $3N_s \times 1$ current and next state vectors corresponding to the proportion of each SOC, respectively, and $y(k)$ is the total output power of the EV aggregator.

The matrix $\mathbf{A}$ is the state transition matrix that can be obtained by estimation method or analytical method [10]. Matrices $\mathbf{B}$ and $\mathbf{C}$ are the constant matrices corresponding to control signals of RegUp and RegDn, as given in Eqns (2)-(3).

Vectors $\mathbf{u}$ and $\mathbf{v}$ are the $N_s \times 1$ input vectors corresponding to the proportion of each SOC. A positive element in $\mathbf{u}$ means the EV aggregator will switch part of the EVs in the corresponding status from charging to idle. In contrast, the negative element means changing from idle to charging. Similarly, a positive element in $\mathbf{v}$ means part or all of the EVs in the corresponding state will be switched from idle to discharging. In contrast, the negative element means changing from discharging to idle. The computation of $\mathbf{u}$ and $\mathbf{v}$ is discussed in the next subsection.

$$\mathbf{B} = [-\mathbf{I}_{1\times N_s}, \mathbf{I}_{1\times N_s}, \mathbf{0}_{1\times N_s}]^T \tag{2}$$

$$\mathbf{C} = [\mathbf{0}_{1\times N_s}, -\mathbf{I}_{1\times N_s}, \mathbf{I}_{1\times N_s}]^T \tag{3}$$

The matrix $\mathbf{D}$ is the constant matrix corresponding to output power as given in Eqn (4).

$$\mathbf{D} = P_{\text{ave}} N_e [-\mathbf{1}_{1\times N_s}, \mathbf{0}_{1\times N_s}, \mathbf{1}_{1\times N_s}] \tag{4}$$

where N_e is the estimated online EV numbers and P_{ave} is the estimated average charging power of the EVs. N_e and P_{ave} can be obtained from the EV charging station operation history data, and the computation error can be bounded by updating periodically [10].

Further, the upper and lower bound of the EV aggregator power can be described below:

$$\begin{cases} \overline{y_{(k)}} = P_{\text{ave}} N_e \cdot \mathbf{1}_{3\times N_s} \cdot \mathbf{x}(k) \\ \underline{y_{(k)}} = -P_{\text{ave}} N_e \cdot \mathbf{1}_{3\times N_s} \cdot \mathbf{x}(k) \end{cases} \tag{5}$$

With the state space modeling, the control signal computation and communication are significantly simplified because the EV aggregator deals with a state vector of a large population of EVs rather than every single EV.

B. Charging Time Constrained SFR Capacities Estimation

Charging time anxiety of EV has drawn interest [14] [15] [16], the increased charging time incurred by AGC response can impede EV owners participating in SFR program. Therefore, the charging time should be considered to follow the EV owners' tolerance of the increased charging time.

When a large EV population is plugged in, there can be a gap between the demanded energy and the charging energy during the charging period. As a result, the gap allows EVs to provide frequency regulation services while not increasing charging time. For a single EV, Eqn (6) describes the available energy for frequency support that secures the EV owner's charging anxiety, where t_{tol} is the EV owner's tolerance of increased charging time.

$$E_a = (t_f - t_s + t_{\text{tol}}) \cdot P_c - (SOC_d - SOC_i) \cdot Q \tag{6}$$

Given the condition that the departure time t_f is challenging to access in practice, Eqn (6) can be further revised for the EV aggregator application,

$$E_a^{'} = (t_{\text{stay,ave}} + t_{\text{tol}}) \cdot P_{\text{ave}} - (SOC_d - SOC_i) \cdot Q_{\text{ave}} \tag{7}$$

where $t_{\text{stay,ave}}$ is the average time of EV staying connected in the charging station, and Q_{ave} is the average capacity. Similar to N_e and P_{ave}, $t_{\text{stay,ave}}$ and Q_{ave} can also be obtained from of EV charging station operation data.

TABLE I
AGC POWER FROM SINGLE EV

P_r \ Status / SOC	Charging	Idle	Discharging
$SOC < SOC_d$	0	P_{u}	$2P_{\text{u}}$
$SOC \geq SOC_d$	$-P_{\text{u}}$	0	P_{u}

Before integrating the charging time constraints, the assumptions for EV in this study are listed below:

- An EV is set to charging status when it connects to the charger.
- The EV owner will input the tolerance of charging time t_{tol} into the charger.
- The EV owner will input the demand SOC level SOC_d to the charger.
- The EV will be switched to idle status if it has been charged to the demand SOC level.

Since the time length of the AGC interval is fixed, the response power P_r from a single EV in an AGC interval is listed in Table I, where $P_{\text{u}} = P_{\text{ave}} \cdot T_{\text{agc}}$ is the unit power of AGC response from one single EV during an AGC interval. EVs that have not been charged to SOC_d are supposed to be in charging status, and thus the EVs in idle and discharging status are considered to be providing AGC response power. Similarly, EVs charged to SOC_d are supposed to be idle; thus, the EVs in charging and discharging status are considered to provide AGC response power.

Eqn (8) translates the available energy $E_a^{'}$ into an action number limit of AGC response. The counter is updated after every AGC interval by $N_a = N_a + P_r/P_{\text{unit}}$, and once the maximum action number is reached, the EV will be out of SFR service.

$$\overline{N_a} = \frac{E_a^{'}}{P_{\text{ave}} \cdot T_{\text{agc}}} \tag{8}$$

In this way, the charging time constraints can be realized by installing a counter locally in each charger, and thus there is no extra communication burden between the charging center and the charger. In addition, the increased charging time can be estimated by the counter as $t_{\text{ICT}} = N_a/\overline{N_a}$.

Then, the number of online EVs N_e in Eqns (4)-(5) should be replaced with N_c which represents the number of in-service EVs.

Further, the charging time-constrained SFR capacities can be estimated by Eqn (9):

$$\begin{cases} \overline{R_e^U} = \overline{y_{(k)}} - y(k) \\ \overline{R_e^D} = y(k) - \underline{y_{(k)}} \end{cases} \tag{9}$$

where $\overline{R_e^U}$ and $\overline{R_e^D}$ are the estimated RegUp and RegDn capacities from the EV aggregator, respectively.

C. Real-time AGC Power Delivery Control

EV aggregator participates in the SFR in two stages: dispatch in RTED and real-time delivery in real-time. By Eqn (9), the power grid control center can procure the regulation capacities from EV as discussed in Section III-A. Then, in the

real-time operation, the EV aggregator delivers the assigned signal. The real-time AGC power delivery is illustrated below:

1) The power signals for each status of the EV are computed as follows:

If $P_{\text{ev}} - P_{\text{rt}} \geq 0$:

$$\begin{cases} r_u = min(P_i,\ P_a)/(P_{\text{ave}} \cdot N_c) \\ u_j = min(r_u - \sum_{h=j+1}^{N_s} x_h - \sum_{h=j+1+N_s}^{2N_s} x_h,\ x_j) \\ r_v = max(P_i - P_a,\ 0)/(P_{\text{ave}} \cdot N_c) \\ v_j = min(r_v - \sum_{h=j+1}^{N_s}(x_{h+N_s} + u_h),\ x_{j+N_s} + u_j) \end{cases} \tag{10}$$

Else if $P_{\text{ev}} - P_{\text{rt}} < 0$:

$$\begin{cases} r_v = max(P_i,\ P_c)/(P_{\text{ave}} \cdot N_c) \\ v_j = max(r_v + \sum_{h=1}^{j-1}(x_{h-1+2N_s}),\ -x_{j+2N_s}) \\ r_u = min(P_i - P_c,\ 0)/(P_{\text{ave}} \cdot N_c) \\ u_j = max(r_u - \sum_{h=1}^{j} v_h - \sum_{h=1}^{j-1} u_h,\ -x_{j+N_s}) \end{cases} \tag{11}$$

where $j = [1, ..., N_s]$, P_{ev} is the AGC power assigned to the EV aggregator, and P_{rt} is the AGC power from the EV aggregator that can be summarized from all the response power P_r from every single EV as listed in the Table I.

2) The power signals for each EV status are translated into probabilities as follows:

If $P_{\text{ev}} - P_{\text{rt}} \geq 0$:

$$\begin{cases} u_{s,j} = min(u_j/x_j,\ 1) \\ v_{s,j} = min(v_j/(x_{j+N_s} + u_j),\ 1) \end{cases} \tag{12}$$

Else if $P_{\text{ev}} - P_{\text{rt}} < 0$:

$$\begin{cases} v_{s,j} = min(-v_j/(x_{j+2N_s} + u_j),\ 1) \\ u_{s,j} = min(-u_j/x_{j+N_s} - v_j,\ 1) \end{cases} \tag{13}$$

3) The probabilities signals from 2) are supplemented with direction signals as the following:

$$\begin{cases} u_{s,N_{s+1}} = v_{s,N_{s+1}} = 1,\ P_{\text{ev}} - P_{\text{rt}} \geq 0 \\ u_{s,N_{s+1}} = v_{s,N_{s+1}} = -1,\ P_{\text{ev}} - P_{\text{rt}} < 0 \end{cases} \tag{14}$$

4) The signals from Eqns (12)-(14) are broadcast to all the EVs, and each single EV will generate a number n locally, where $n \sim U(0, 1)$. The action is then determined by comparing the number n with the corresponding status p:

$$\begin{cases} \text{switch},\ n \geq p \\ \text{stay},\ n < p \end{cases} \tag{15}$$

The overall workflow of the EV aggregator is summarized in the Algorithm 1, where $N \in N_0$, T_{ed} is the cycle time of RTED, T_p is the update cycle time of EV aggregator, and T_{agc} is the AGC cycle time.

Algorithm 1 EV Aggregator Control

```
Initialize EV aggregator
for t in T_total
    if t = N · T_ed
        Estimate SFR capacities with Eqn (9);
    if t = N · T_p
        Record x and update A;
    if t = N · T_agc
        Compute signals with Eqns (10)-(14);
    Run Monte Carlo simulation;
    Switch EVs with Eqn (15);
    Estimate x and y with Eqn (1);
```

III. Procurement and Delivery of SFR from EV

This section introduces the procurement of EV SFR capacity in the RTED and the RTED-TDS co-simulation framework used to verify the proposed strategy.

A. Procurement of EV SFR in the RTED

The procurement of EV SFR ($R^U_{e,t}$ and $R^D_{e,t}$) in the RTED requires the EV aggregator to provide available SFR capacities $\overline{R^U_e}$ and $\overline{R^D_e}$. Given the EV uncertainties are addressed by the EV aggregator, the RTED can be modeled as below, where the variables are explained in the Nomenclature:

$$\min \sum_{t\in\Omega_T} \left(\sum_{i\in\Omega_G} \left(f_{g,t}\left(P^{\text{sch}}_{g,t}\right) + c^U_{g,t}R^U_{g,t} + c^D_{g,t}R^D_{g,t}\right) + \sum_{i\in\Omega_E} \left(c^U_{e,t}R^U_{e,t} + c^D_{e,t}R^D_{e,t}\right) \right), \forall g \in \Omega_G, \forall e \in \Omega_E \tag{16}$$

s.t.

$$\Delta D^U_t = \sum_{g\in\Omega_G} R^U_{g,t} + \sum_{e\in\Omega_E} R^U_{e,t} \tag{17}$$

$$\Delta D^D_t = \sum_{g\in\Omega_G} R^D_{g,t} + \sum_{e\in\Omega_E} R^D_{e,t} \tag{18}$$

$$\sum_{b\in\Omega_B} P^{\text{sch}}_{g,t} - \sum_{b\in\Omega_B} D_b = 0 \tag{19}$$

$$P^{\text{sch}}_{g,t} + R^U_{g,t} \leq \overline{P_g}, \forall g \in \Omega_G, \forall t \in \Omega_T \tag{20}$$

$$\underline{P_g} \leq P^{\text{sch}}_{g,t} - R^D_{g,t}, \forall g \in \Omega_G, \forall t \in \Omega_T \tag{21}$$

$$R^U_{e,t} \leq \overline{R^U_e}, \forall e \in \Omega_E, \forall t \in \Omega_T \tag{22}$$

$$R^D_{e,t} \leq \overline{R^D_e}, \forall e \in \Omega_E, \forall t \in \Omega_T \tag{23}$$

$$P_{g,t} - P_{g,t-1} \leq \rho^U_g \cdot \Delta t, \forall i \in \Omega_G, \forall t \in \Omega_T \tag{24}$$

$$P_{g,t-1} - P_{g,t} \leq \rho^D_g \cdot \Delta t, \forall i \in \Omega_G, \forall t \in \Omega_T \tag{25}$$

$$-\overline{P_{l,k}} \leq P_{l,k} \leq \overline{P_k}, \forall k \in \Omega_K \tag{26}$$

The underline and overline of the variables represent the minimum and maximum, respectively. Superscripts U and D represents regulation up and down, respectively. Eqn (16) is the objective function; Eqns (17) - (18) represent the SFR equality constraints; Eqn (19) represents the power balance; Eqns (20) - (21) are the minimum/maximum output of conventional units; Eqns (22) - (23) are the minimum/maximum SFR output of the EV aggregator, where the $R^U_{e,t}$ and $R^D_{e,t}$ are estimated from the EV aggregator as described in the previous subsection II-C; Eqns (24) - (25) are the ramping up/down limits of conventional units; Eqn (26) represents the line thermal limits. In the RTED modeling, the decision variables are $P^{\text{sch}}_{g,t}$, $R^U_{g,t}$, $R^D_{g,t}$, $R^U_{e,t}$, $R^D_{e,t}$.

Once the SFR capacities are settled down, the participation factor of each AGC unit is determined by the ratio of its SFR capacity out of the total demanded SFR capacity, as shown in Eqns (27)-(28):

$$\beta^U_{g,t} = R^U_{g,t}/\Delta D^U_t, \forall g \in \Omega_G \cup \Omega_E, \forall t \in \Omega_T \tag{27}$$

$$\beta^D_{g,t} = R^D_{g,t}/\Delta D^D_t, \forall g \in \Omega_G \cup \Omega_E, \forall t \in \Omega_T \tag{28}$$

where the $\beta^U_{g,t}$ and $\beta^D_{g,t}$ are the RegUp and RegDn participation factors of each AGC unit, respectively.

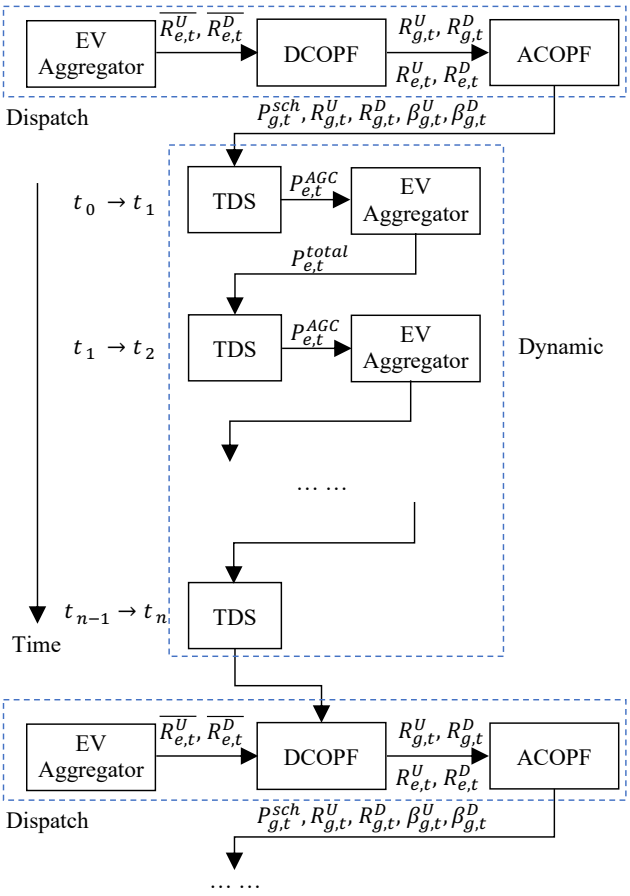

Fig. 1. Framework of RTED-TDS co-simulation

B. RTED-TDS Co-Simulation Framework

RTED-TDS co-simulation is proposed to simulate the close-loop AGC control on the area level. The complete frequency regulation study includes the dispatch results and the dynamic process. However, there can be a gap when applying the RTED solution to the TDS. In the RTED-related problem formulation, DCOPF or the linearized ACOPF can be used, while the ACOPF is used to initialize the TDS. The gap results from DCOPF or linearized ACOPF ignoring the voltage range and the power loss, and then the slack generator will compensate for the unbalanced power. As a result, the scheduled generation is broken, and the TDS initialization can fail because of the divergence of ACOPF. Therefore, to reduce the modeling complexity and guarantee a smooth transition from dispatch to dynamic, a DC-AC hybrid OPF structure is proposed. The design of DCOPF and ACOPF hybrid solutions allows the extensibility to other dispatch formulations, such as unit commitment problems. In this design, DCOPF enables rapid prototyping of dispatch problems, while ACOPF secures the consistency and initialization of the TDS.

Figure 1 illustrates the proposed framework of RTED-TDS co-simulation. The framework coordinates four entities: EV Aggregator is the proposed charging time-constrained EV aggregator, DCOPF stands for the DCOPF-based dispatch simulator, ACOPF represents the ACOPF-based dispatch simulator, and TDS is the dynamic simulator. The dispatch simulator involves the DCOPF, and ACOPF implemented with gurobipy and pandapower [18], respectively. The dynamic simulation is powered by the open-source simulation engine LTB ADNES [19], [20]. The data is federated between the EV aggregator and the dynamic model [21] to capture the EV dynamics. The four entities are grouped into two modules, i.e., dispatch and dynamic, and the two modules are iterated to perform the co-simulation.

The dispatch module contains three steps. First, the available SFR capacities from the EV aggregator and other AGC units are reported to the control center. Second, the procurement of SFR ($R^U_{g,t}$, $R^D_{g,t}$, $R^U_{e,t}$, $R^D_{e,t}$) is solved with DCOPF-based RTED model as described in the section III-A. However, the setting points $P^{\text{sch}}_{g,t}$ solved from DCOPF can result in a mismatch in the TDS. Third, therefore, setting points $P^{\text{sch}}_{g,t}$ are re-solved from ACOPF [22] to secure the initialization of TDS and the accuracy of the dispatch results. The SFR capacities and the ramping limits from the first step are reserved by adjusting the generator limits, as shown in Eqns (29)-(30).

$$\overline{P'_g} = min(\overline{P_g} - R^U_{g,t}, \overline{P_g} - \rho^U_g \cdot \Delta t) \tag{29}$$

$$\underline{P'_g} = max(\underline{P_g} + R^D_{g,t}, \underline{P_g} + \rho^U_g \cdot \Delta t) \tag{30}$$

Once the dispatch results are settled, the dynamic module will run the TDS by iterating ANDES and the EV aggregator. The iteration involves two steps. First, the TDS will run to set end time $t_{0,0}$ and generate the AGC signal $P^{\text{AGC}}_{e,t}$ of the EV aggregator. Second, the EV aggregator responds to the AGC signal while running to the same end time $t_{0,0}$. Then the two steps are iterated till the end of the first dynamic period.

After the dynamic simulation, in the following dispatch period, the dynamic results will be reported to the control center as the start point.

The secondary frequency regulation on the area level is implemented in the area-level area control error (ACE) model and the plant-level automatic generation control (AGC) model. The area-level ACE represents the system power imbalance and is defined by North America Electric Reliability Corporation [1]. With the ignorance of interchange (tie line) metering error, it can be calculated with Eqn (31), where β is the system bias factor (MW/0.1Hz), f and f_n are the measured and nominal frequency (Hz), respectively, P_{tl} and $P^{\text{sch}}_{\text{tl}}$ are the actual tie line power (MW) and the scheduled tie line power (MW), respectively.

$$ACE = 10\beta(f - f_n) + (P_{\text{tl}} - P^{\text{sch}}_{\text{tl}}) \tag{31}$$

Taking ACE as the input signal, the plant-level AGC model will generate auxiliary power signal P_{aux}, as illustrated in Figure 2, where K_p and K_i are the gain and integral constants of the PI controller, respectively.

In the power system operation, the SFR mileage calculation must be necessary. The actual SFR mileages of EV aggregator are similar to conventional generators, as given in Eqn (32):

$$P_{\text{mile},i_{\text{ed}}} = \sum_{i_{\text{agc}}=1}^{N_{\text{agc}}-1} |P_{\text{agc},i_{\text{agc}}+1,i_{\text{ed}}} - P_{\text{agc},i_{\text{agc}},i_{\text{ed}}}| \tag{32}$$

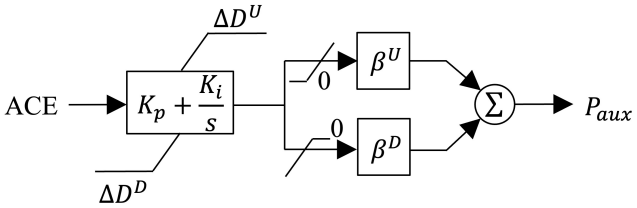

Fig. 2. AGC unit control

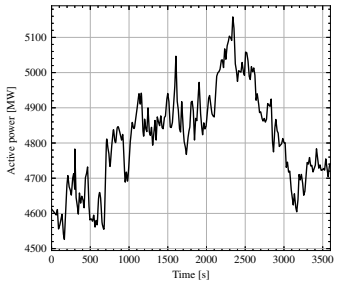

Fig. 3. System load curve

where $P_{\text{mile},i_{\text{ed}}}$ is the mileage of EV aggregator of the $i_{\text{ed}}th$ RTED interval, $P_{\text{agc},i_{\text{agc}},i_{\text{ed}}}$ means the AGC power of EV aggregator of the $i_{\text{agc}}th$ AGC interval in the $i_{\text{ed}}th$ RTED interval.

Algorithm 2 RTED-TDS Co-Simulation

```
1: Initialize EV aggregator, DCOPF, ACOPF, TDS
2: for t in T_total
3:     if t = N · T_ed
4:         EV aggregator: estimate SFR with Eqn (9);
5:         DCOPF: update info from dynamic;
6:                solve RTED with Eqns (16)-(28);
7:         ACOPF: resolve with Eqns (29)-(30);
8:         TDS: assign schedule results from ACOPF;
9:     if t = N · T_agc
10:        TDS: assign AGC power;
11:        EV Aggregator: run with Algorithm 1;
12:    TDS: federate power from EV aggregator;
13:        run TDS;
14:        compute ACE with Eqn (31);
```

As illustrated in the Algorithm 2, lines 4-8 are the dispatch module, and lines 10-14 are the dynamic module. The detailed data federation is listed below:

1) line 4: the available SFR capacities from EV are computed with Eqn (9) and updated into Eqns (23)-(22) of TDS;
2) line 6: the previous setting points P_g^{t-1} of Eqns (20)-(21) of TDS are replaced with actual output power from TDS results;
3) line 8 the setting points calculated from ACOPF are updated into corresponding generation units in TDS;
4) line 12: the output power of the EV Aggregator is updated into the EV dynamic model in TDS.

IV. Case Studies

For verification and demonstration, this section carries out case studies using the proposed RTED-TDS co-simulation. The IEEE 39-bus system is modified to demonstrate the potential of EVs participating in SFR with the proposed charging time-constrained aggregator modeling.

A. Simulation Settings

All studies are performed on a laptop with Apple M1 processors and 16 GB RAM. The environment of the EV aggregation algorithm and the RTED-TDS co-simulation is deployed in Python 3.9 with ANDES 1.7.

The parameters of EV traveling behaviors are derived from [10], and the EV aggregator parameters are set as follows: step size $T_e = 1s$, SOC intervals $N_s = 20$, and update cycle $T_p = 40s$. The step size of the co-simulation is set as $T_c = 1s$. The heaviest charging load occurs around 6 PM [17], and the average SOC level is relatively low than other periods. Thus, the scenario at 6 PM was chosen to demonstrate the secured charging demand and the potential of aggregated EVs participating in SFR provision with charging time constraints.

The load profile is synthesized from PJM load data [23], as depicted in Figure 3.

B. EV Aggregator Modeling Validation

In the TDS, there are two approaches to modeling EV dynamics. First, we can model every EV to secure the simulation accuracy, marked as M1. However, this detailed modeling in M1 can bring a heavy computation burden when the EV number is significant. To address this issue, the second approach is to aggregate the large number of EVs into one single dynamic EV device, with the output power set to track the total output power of all EVs, marked as M2. Note that, with the aggregated M2, although some details, such as each EV's SOC and output power, are excluded in the TDS, these detailed individual EV operational parameters are calculated in the separated EV aggregator model.

IEEE 39-bus system with EV dynamic devices is used to validate the accuracy of the M2 model. In the benchmark test, M1 includes all the 1,000 EV dynamic devices in the TDS, while M2 only contains one.

The 50s simulation under a generation trip contingency consumes 3.400s using M1 versus 2.237s using M2. The 1200s simulation under regular operation consumes 895s using M1 versus 172s using M2. Figure 4 shows the system's dynamic responses. From the above results, it can be seen that M2 significantly accelerates the simulation while reserving EV information with high accuracy. Therefore, M2 is used in this study to investigate the aggregated EV providing SFR.

C. IEEE 39-Bus System

As visualized using LTB AGVis [24] in Figure 5, IEEE 39-bus system is modified to include an EV aggregator with a total of 50,000 EVs.

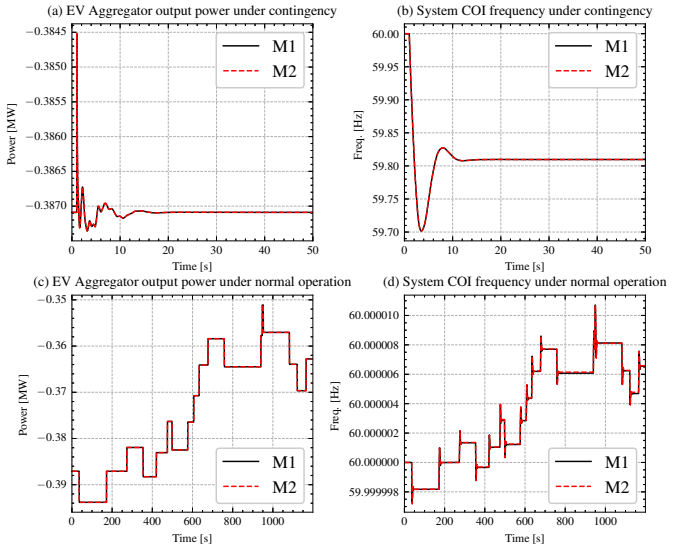

Fig. 4. Benchmark of EV modeling (a) Total power under normal operation; (b) System frequency under normal operation; (c) Total power under generator tripping; (d) System frequency under generator tripping.

TABLE II
IEEE 39-BUS SYSTEM GENERATION PARAMETERS

Unit	Cost ($/MW)				Pmax	Pmin	Ramp
	a	b	c	SFR	(MW)	(MW)	(MW/5 min)
G1	0.0140	20	500	0	10.4	4.16	52
G2	0.0200	20	380	0	6.46	2.58	40
G3	0.0194	20	42	0	7.25	2.9	43.33
G4	0.0200	20	380	0	6.52	2.6	36.67
G5	0.0255	20	295	0	5.08	2.0	26.67
G6	0.0210	20	400	0	6.87	2.74	35
G7	0.2300	20	350	0	5.8	2.32	30
G8	0.2220	20	330	0	5.64	2.256	30
G9	0.0150	20	490	0	8.65	3.64	50
G10	0.1400	20	500	0	11	4.4	66.67

The generation parameters [25] are listed in Table II. Referenced from ISO-NE, the mileage price is set as 0.99$/MWh, and the penalty of extra increased charging time is set as 4$/h. Three cases listed below are tested to demonstrate the charging time-constrained EV aggregator modeling:

- Case1: EV not providing SFR
- Case2: EV providing SFR without charging time constraints
- Case3: EV providing SFR with charging time constraints

The simulation results are shown and interpreted in the following subsections.

D. EV Aggregator Results

Figure 6 illustrates the EV Aggregator response of Case2 and Case3. It can be seen that the AGC power assigned to the EV aggregator is delivered accurately. Noted that, Case1 is not included in Figure 6 because in Case1 EV aggregator has zero control and response signal. This is also the case for Figure 8.

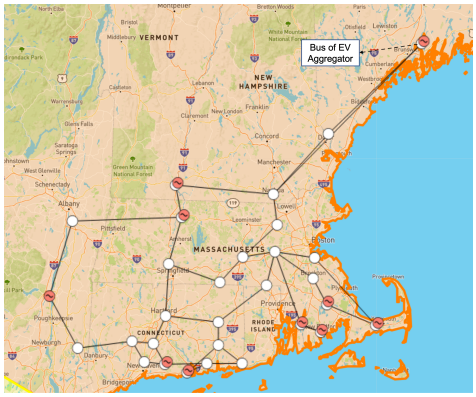

Fig. 5. IEEE 39-bus system topology visualized by LTB AGVis

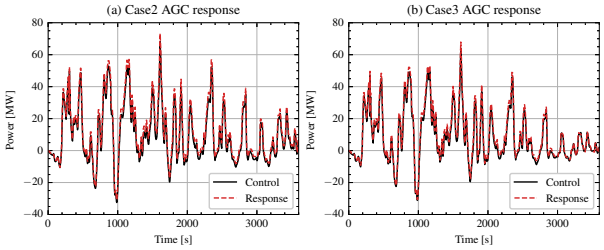

Fig. 6. EV aggregator response

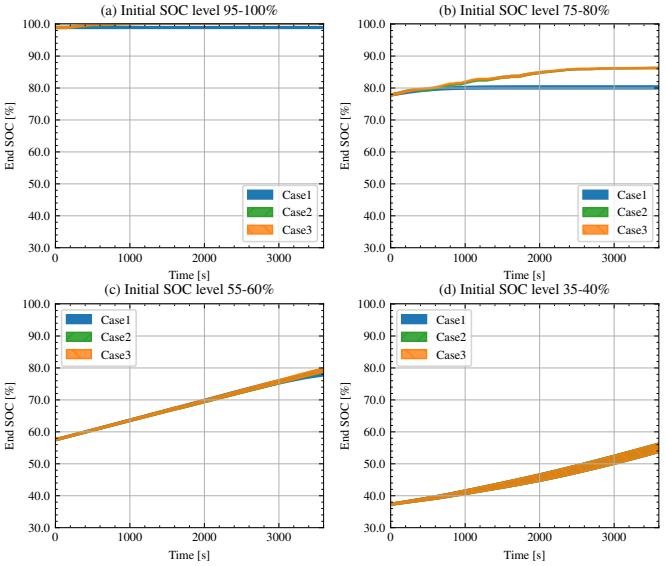

Fig. 7. 95% confidence interval of ended SOC by a group of initial SOC

Figure 7 depicts the 95% confidence interval of the EV SOC curve by four groups of different initial SOC levels. In Figure 7 (a) and (b), EVs that have been charged to the desired SOC level are still charged in Case2 and Case3, whereas in Case1, they remained unchanged. RegDn power is withdrawn from switching idle EVs to charging, where EVs already charged to demanded SOC are usually in idle status. When comparing Figure 7(c) and (d) versus (a) and (b), it can be seen that the control strategy can secure the charging demand of EVs

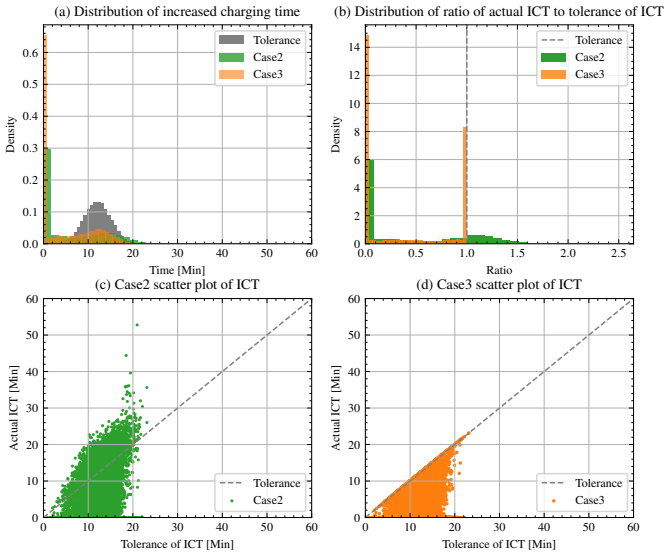

Fig. 8. EV increased charging time

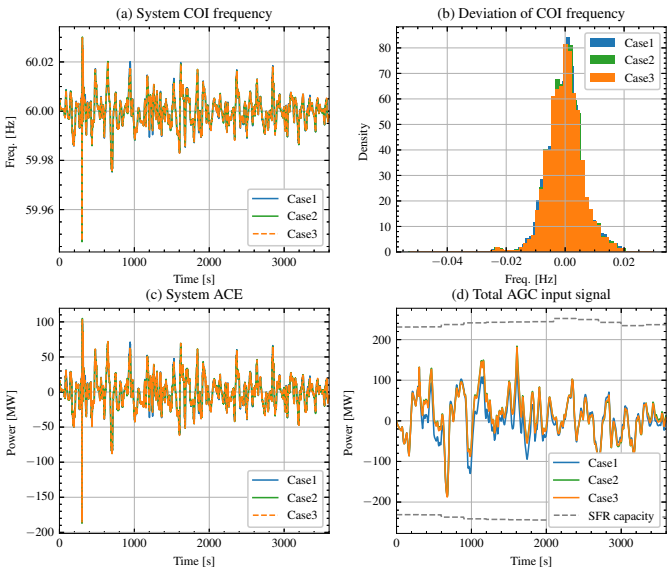

Fig. 9. System dynamic results

with lower initial SOC levels. Figure 7 shows that the EV aggregator control strategy can secure EV charging demand.

Figure 8 illustrates the increased charging time of Case2 and Case3. In Figure 8(a), the distribution shape of Case3 is similar to that of the tolerance, while Case2 is out of the tolerance range. Further, Figure 8(b) shows the ratio of actual increased charging time to the tolerance for every EV. In Case 2, parts of EVs exceed the tolerance, while the tolerance in Case 3 limits the increased charging times. In addition, the scatter plots of increased charging time in Figure 8(c) and (d) shows again that the tolerance of increased charging time is violated in Case2 but obeyed in Case3. Figure 8 verifies that the tolerance of charging time constraints is followed well using the proposed charging time constraints.

E. System results

Figure 9 depicts the system dynamic results. Figure 9(a) illustrates the system COI frequency. The spikes of Case2 and Case3 are slightly lower than that in Case1, but Case2 and Case3 are almost overlapped. A similar condition can be seen from the distribution of the COI frequency as shown in Figure 9(b). The distribution of the COI frequency deviation is more concentrated in Case2 and Case3 than in Case1, and the variation is slightly more concentrated in Case3 than Case2. Figure 9(c) shows the system ACE. This figure is similar to Figure 9(a) because the test system is controlled as one area. Figure 9(d) displays the total AGC input signal of the system, where the dashed lines represent the SFR capacity. The figure indicates that the SFR capacities are sufficient in all three test cases. However, when comparing Case2 and Case3 versus Case1, it can be found that when EV provides SFR, the system assigns more RegDn power while less RegUp power.

To be more specific, Table III shows the metrics of system frequency regulation. When looking at the CPS1 score, it can be found that EV providing SFR enhances the CPS1 score by comparing Case2 and Case3 versus Case1. In addition, Case2 and Case3 consumed more AGC mileage than Case1. Comparing Case2 versus Case3 shows that their dynamic performance is close, although, in Case3, the charging time constraints slightly degraded the frequency metrics. In summary, Table III indicates that EV providing SFR slightly enhanced the system dynamic performance while consuming more AGC mileage. The charging time constraints of EV aggregators bring a few impacts on the system's dynamic performance.

TABLE III
SYSTEM FREQUENCY REGULATION METRICS

	Case1	Case2	Case3
Freq. Dev. mean [Hz]	0	0.00001	0.00001
Freq. Dev. Std. [Hz]	0.00623	0.00600	0.00603
ACE mean [MW]	-0.01521	-0.0522	-0.03912
ACE Std. [MW]	21.77829	20.97947	21.07158
CPS1 score	153.08869	156.70854	156.26189
AGC mileage [MWh]	8277.79918	8940.76994	8864.53066
EV AGC mileage[MWh]	0	2043.33919	1801.41695

The balancing factors of the three cases are illustrated in Figure 10. When comparing Case2 and Case3, it can be seen that the balancing factors of the EV aggregator in Case3 are lower than that of Case2 for both RegUp and RegDn. This indicated that the charging time constraints resulted in a decrease in frequency regulation capacities.

Table IV shows the system's economic results. When comparing Case2 and Case3 versus Case1, it can be seen that EV-providing SFR reduces the system generation cost. This is caused by the decreased load from the EV charging station when EV provides SFR. Consistent with AGC mileage in Table III, EV participating SFR results in higher mileage payment, and the mileage payment of Case3 is close to Case2. Regarding the compensation for extra increased charging time, by comparing Case 2 versus Case 3, it should be noticed

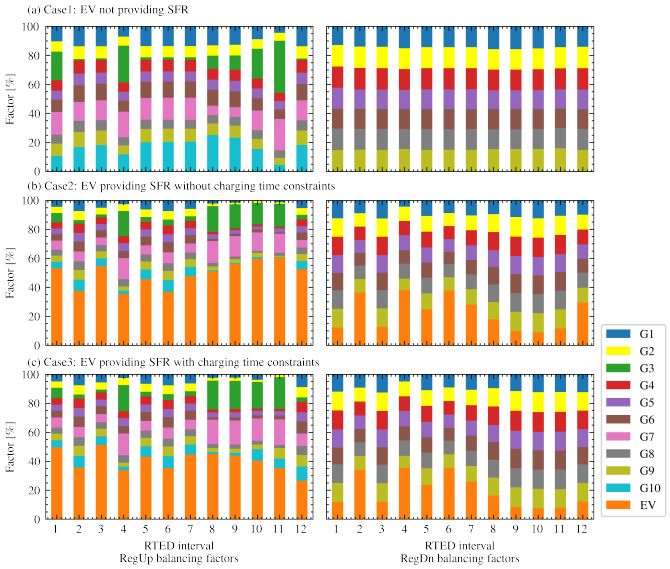

Fig. 10. System balancing factors

TABLE IV
SYSTEM ECONOMIC RESULTS

	Case1	Case2	Case3
Generation cost [$]	133,031.395	132,500.647	132,556.211
Mileage payment [$]	8,195.021	8,851.362	8,775.885
Mileage payment to EV [$]	0	2,022.906	1,783.403
ICT compensation to EV [$]	0	846.1502	0.00087
System total cost [$]	141,226.416	142,198.159	141,332.097

that there is almost zero compensation in Case 3. Further, the system total cost shows that Case3 is lower than Case2 while close to Case1. Table IV implies that EV aggregators with charging time constraints have limited impacts on the system's economic performance.

In summary, the Case Studies demonstrate the benefits of charging time-constrained EV aggregation providing SFR. First, the reliable real-time delivery of the EV aggregator proving SFR is verified. Second, the system's dynamic performance is improved with a slightly increased total cost. Third, the increased charging time is secured with the proposed charging time constraints.

V. CONCLUSION

In conclusion, this paper proposes an EV charging time-constrained deliverable SFR provision model. First, the state space modeling addresses the uncertainties from EV heterogeneous parameters and traveling behaviors. The EV owner's preference translation respects the charging time into a real-time AGC activation limiter for the individual EV. Second, inter-interval SFR reserve procurement is facilitated by estimating EV SFR capacities, and the EV aggregation strategy reliably delivers real-time intra-interval AGC response. Third, a hybrid OPF structure is proposed in the RTED-TDS co-simulation to evaluate the economic and reliability performance of EV aggregation's SFR provision. The proposed structure can secure the broadcasting dispatch results into the dynamic simulation, reducing the overall co-simulation modeling complexity. Last, the proposed charging time-constrained EV aggregation is verified using the RTED-TDS co-simulation framework on IEEE 39-bus system. Results indicate that the proposed model can improve the system's dynamic performance and respect the EV owners' tolerance of increased charging time.

ACKNOWLEDGMENTS

The authors would like to acknowledge the financial support from CURENT, a National Science Foundation (NSF) Engineering Research Center funded by NSF and the Department of Energy under NSF Award EEC-1041877.

This work was partly authored by the National Renewable Energy Laboratory, operated by Alliance for Sustainable Energy, LLC, for the U.S. Department of Energy (DOE) under Contract No. DE-AC36-08GO28308. The U.S. Department of Energy Office of Electricity Advanced Grid Research and Development program provides funding. The U.S. Government retains, and the publisher, by accepting the article for publication, acknowledges that the U.S. Government retains a nonexclusive, paid-up, irrevocable, worldwide license to publish or reproduce the published form of this work or allow others to do so for the U.S. Government purposes. The views expressed in the article do not necessarily represent the views of the DOE or the U.S. Government.

REFERENCES

[1] NERC, *Ancillary service and balancing authority area solutions to integrate variable generation*, Mar. 2011.

[2] N. Gao, D. W. Gao, and X. Fang, "Manage real-time power imbalance with renewable energy: Fast generation dispatch or adaptive frequency regulation?" *IEEE Transactions on Power Systems*, pp. 1–12, 2022.

[3] C. Ning and F. You, "Data-driven adaptive robust unit commitment under wind power uncertainty: A bayesian nonparametric approach," *IEEE Transactions on Power Systems*, vol. 34, no. 3, pp. 2409–2418, May 2019.

[4] G. Zhang, E. Ela, and Q. Wang, "Market scheduling and pricing for primary and secondary frequency reserve," *IEEE Transactions on Power Systems*, vol. 34, no. 4, pp. 2914–2924, Jul. 2019.

[5] X. Fang, H. Yuan, and J. Tan, "Secondary frequency regulation from variable generation through uncertainty decomposition: An economic and reliability perspective," *IEEE Transactions on Sustainable Energy*, vol. 12, no. 4, pp. 2019–2030, Oct. 2021.

[6] W. Kempton and J. Tomić, "Vehicle-to-grid power implementation: From stabilizing the grid to supporting large-scale renewable energy," *Journal of Power Sources*, vol. 144, no. 1, pp. 280–294, Jun. 2005.

[7] C. Liu, K. T. Chau, D. Wu, and S. Gao, "Opportunities and challenges of vehicle-to-home, vehicle-to-vehicle, and vehicle-to-grid technologies," *Proceedings of the IEEE*, vol. 101, no. 11, pp. 2409–2427, Nov. 2013.

[8] M. Gonzalez Vaya and G. Andersson, "Self scheduling of plug-in electric vehicle aggregator to provide balancing services for wind power," *IEEE Transactions on Sustainable Energy*, vol. 7, no. 2, pp. 886–899, Apr. 2016.

[9] K. Kaur, M. Singh, and N. Kumar, "Multiobjective optimization for frequency support using electric vehicles: An aggregator-based hierarchical control mechanism," *IEEE Systems Journal*, vol. 13, no. 1, pp. 771–782, Mar. 2019.

[10] M. Wang, Y. Mu, F. Li, *et al.*, "State space model of aggregated electric vehicles for frequency regulation," *IEEE Transactions on Smart Grid*, vol. 11, no. 2, pp. 981–994, Mar. 2020.

[11] S. Kiani, K. Sheshyekani, and H. Dagdougui, "An extended state space model for aggregation of large-scale EVs considering fast charging," *IEEE Transactions on Transportation Electrification*, pp. 1–1, 2022.

[12] T. Kerci and F. Milano, "A framework to embed the unit commitment problem into time domain simulations," in *2019 IEEE International Conference on Environment and Electrical Engineering and 2019 IEEE Industrial and Commercial Power Systems Europe (EEEIC / I&CPS Europe)*, Genova, Italy: IEEE, Jun. 2019, pp. 1–5.

[13] T. Kerci, M. A. A. Murad, I. Dassios, and F. Milano, "On the impact of discrete secondary controllers on power system dynamics," *IEEE Transactions on Power Systems*, vol. 36, no. 5, pp. 4400–4409, Sep. 2021.

[14] D. Knutsen and O. Willén, *A study of electric vehicle charging patterns and range anxiety*, Jun. 2013.

[15] A. Alsabbagh, B. Wu, and C. Ma, "Distributed electric vehicles charging management considering time anxiety and customer behaviors," *IEEE Transactions on Industrial Informatics*, vol. 17, no. 4, pp. 2422–2431, Apr. 2021.

[16] L. Yan, X. Chen, J. Zhou, Y. Chen, and J. Wen, "Deep reinforcement learning for continuous electric vehicles charging control with dynamic user behaviors," *IEEE Transactions on Smart Grid*, vol. 12, no. 6, pp. 5124–5134, Nov. 2021.

[17] B. Wang, D. Zhao, P. Dehghanian, Y. Tian, and T. Hong, "Aggregated electric vehicle load modeling in large-scale electric power systems," *IEEE Transactions on Industry Applications*, vol. 56, no. 5, pp. 5796–5810, Sep. 2020.

[18] L. Thurner, A. Scheidler, F. Schafer, *et al.*, "Pandapower—an open-source python tool for convenient modeling, analysis, and optimization of electric power systems," *IEEE Transactions on Power Systems*, vol. 33, no. 6, pp. 6510–6521, Nov. 2018.

[19] H. Cui, F. Li, and K. Tomsovic, "Hybrid symbolic-numeric framework for power system modeling and analysis," *IEEE Transactions on Power Systems*, vol. 36, no. 2, pp. 1373–1384, Mar. 2021, Number: 2.

[20] F. Li, K. Tomsovic, and H. Cui, "A large-scale testbed as a virtual power grid: For closed-loop controls in research and testing," *IEEE Power and Energy Magazine*, vol. 18, no. 2, pp. 60–68, Mar. 2020, Number: 2.

[21] Y. Liu, T. J. Overbye, W. Wang, *et al.*, "Transmission-distribution dynamic co-simulation of electric vehicles providing grid frequency response," in *2022 IEEE Power & Energy Society General Meeting (PESGM)*, Denver, CO, USA: IEEE, Jul. 17, 2022, pp. 1–5.

[22] R. D. Zimmerman, C. E. Murillo-Sanchez, and R. J. Thomas, "MATPOWER: Steady-state operations, planning, and analysis tools for power systems research and education," *IEEE Transactions on Power Systems*, vol. 26, no. 1, pp. 12–19, Feb. 2011.

[23] PJM. "Data miner 2." (), [Online]. Available: https://dataminer2.pjm.com/list.

[24] N. Parsly, J. Wang, N. West, Q. Zhang, H. Cui, and F. Li, "DiME and AGVIS a distributed messaging environment and geographical visualizer for large-scale power system simulation," 2022, Publisher: arXiv Version Number: 1.

[25] J. Li, J. Wen, and X. Han, "Low-carbon unit commitment with intensive wind power generation and carbon capture power plant," *Journal of Modern Power Systems and Clean Energy*, vol. 3, no. 1, pp. 63–71, Mar. 2015.